



## Pressure induced Ag<sub>2</sub>Te polymorphs in conjunction with topological non trivial to metal transition

J. Zhu, A. R. Oganov, W. X. Feng, Y. G. Yao, S. J. Zhang, X. H. Yu, J. L. Zhu, R. C. Yu, C. Q. Jin, X. Dai, Z. Fang, and Y. S. Zhao

Citation: *AIP Advances* **6**, 085003 (2016); doi: 10.1063/1.4960606

View online: <http://dx.doi.org/10.1063/1.4960606>

View Table of Contents: <http://scitation.aip.org/content/aip/journal/adva/6/8?ver=pdfcov>

Published by the *AIP Publishing*

---

### Articles you may be interested in

Pressure induced structural, electronic topological, and semiconductor to metal transition in AgBiSe<sub>2</sub>  
*Appl. Phys. Lett.* **109**, 171903 (2016); 10.1063/1.4966275

Enhanced thermoelectric performance of n-type transformable AgBiSe<sub>2</sub> polymorphs by indium doping  
*Appl. Phys. Lett.* **109**, 133901 (2016); 10.1063/1.4963779

Experimental and theoretical identification of a high-pressure polymorph of Ga<sub>2</sub>S<sub>3</sub> with α-Bi<sub>2</sub>Te<sub>3</sub>-type structure  
*J. Appl. Phys.* **116**, 193507 (2014); 10.1063/1.4902070

Reinvestigation of high pressure polymorphism in hafnium metal  
*J. Appl. Phys.* **115**, 233513 (2014); 10.1063/1.4884436

Polymorphism in pentacene thin films on Si O<sub>2</sub> substrate  
*Appl. Phys. Lett.* **90**, 081903 (2007); 10.1063/1.2709516

---

The advertisement features a blue and orange background with a molecular structure graphic. On the left is a thumbnail of an 'Applied Physics Reviews' journal cover. The main text reads 'NEW Special Topic Sections' in large white font. Below this, it says 'NOW ONLINE' in orange, followed by 'Lithium Niobate Properties and Applications: Reviews of Emerging Trends' in white. The AIP Applied Physics Reviews logo is in the bottom right corner.

**NEW Special Topic Sections**

**NOW ONLINE**  
Lithium Niobate Properties and Applications:  
Reviews of Emerging Trends

**AIP** Applied Physics Reviews

## Pressure induced $\text{Ag}_2\text{Te}$ polymorphs in conjunction with topological non trivial to metal transition

J. Zhu,<sup>1</sup> A. R. Oganov,<sup>2</sup> W. X. Feng,<sup>3</sup> Y. G. Yao,<sup>3</sup> S. J. Zhang,<sup>1,a</sup> X. H. Yu,<sup>1</sup> J. L. Zhu,<sup>4</sup> R. C. Yu,<sup>1</sup> C. Q. Jin,<sup>1,a</sup> X. Dai,<sup>1</sup> Z. Fang,<sup>1</sup> and Y. S. Zhao<sup>1,5</sup>

<sup>1</sup>*Institute of Physics, Chinese Academy of Sciences, Beijing 100190, China*

<sup>2</sup>*Department of Geosciences, University of New York at Stony Brook, USA*

<sup>3</sup>*Department of Physics, Beijing Institute of Technology, Beijing, China*

<sup>4</sup>*High Pressure Science and Engineering Center, University of Nevada, Las Vegas, Nevada 89154, United States*

<sup>5</sup>*South University of Science and Technology of China, Shenzhen, Guangdong, China*

(Received 2 June 2016; accepted 25 July 2016; published online 3 August 2016)

Silver telluride ( $\text{Ag}_2\text{Te}$ ) is well known as superionic conductor and topological insulator with polymorphs. Pressure induced three phase transitions in  $\text{Ag}_2\text{Te}$  have been reported in previous. Here, we experimentally identified high pressure phase above 13 GPa of  $\text{Ag}_2\text{Te}$  by using high pressure synchrotron x ray diffraction method in combination with evolutionary crystal structure prediction, showing it crystallizes into a monoclinic structure of space group  $C2/m$  with lattice parameters  $a = 6.081\text{\AA}$ ,  $b = 5.744\text{\AA}$ ,  $c = 6.797\text{\AA}$ ,  $\beta = 105.53^\circ$ . The electronic properties measurements of  $\text{Ag}_2\text{Te}$  reveal that the topologically non-trivial semiconducting phase I and semi-metallic phase II previously predicated by theory transformed into bulk metals for high pressure phases in consistent with the first principles calculations. © 2016 Author(s). All article content, except where otherwise noted, is licensed under a Creative Commons Attribution (CC BY) license (<http://creativecommons.org/licenses/by/4.0/>). [<http://dx.doi.org/10.1063/1.4960606>]

### I. INTRODUCTION

$\text{Ag}_2\text{Te}$ , which occurs naturally as the mineral hessite, has attracted considerable interest in recent years. It has different polymorphs under standard atmospheric pressure, in which some novel phenomena were observed.<sup>1-9</sup> High temperature fcc ( $\alpha$ ) and bcc ( $\gamma$ ) – structured phases, characterized by the fast-moving  $\text{Ag}^+$  ions, can be used as superionic conductor.<sup>2</sup> When temperature drops below 417 K, it transforms to monoclinic  $\beta\text{-Ag}_2\text{Te}$ , a nonmagnetic semiconductor with a narrow gap in the range of several tens of meV.<sup>3-5</sup> The  $\beta\text{-Ag}_2\text{Te}$  has a high electron mobility<sup>6</sup> and low thermal conductivity<sup>7</sup> and thus is very sensitive to external effects, such as pressure. Lately an anomalously large linear magnetoresistive response was observed in  $\beta\text{-Ag}_2\text{Te}$  from mTesla to Tesla,<sup>8,9</sup> which led to many possible models to explain this novel phenomenon.<sup>10-13</sup> In particular, a quantum scenario was proposed very recently based on the assumption of gapless linear energy spectrum, in which  $\beta\text{-Ag}_2\text{Te}$  was confirmed to be a new kind of possible topological insulator with a highly anisotropic Dirac cone.<sup>13,14</sup> Remarkably, all these unique characteristics mentioned above make  $\text{Ag}_2\text{Te}$  very promising for practical applications as a multi-functional compound.

Pressure, just as temperature and chemical composition, belongs to one of the three fundamental thermodynamic variables. Application of pressure can not only afford considerable insight into understanding the properties of materials, but also modify the atomic structure and the nature of chemical bonds to generate new states of materials.<sup>15-17</sup> For example, electrical and magnetotransport studies on  $\text{Ag}_2\text{Te}$  showed that pressure can significantly influence the electrical resistivity and magnetoresistive (MR) behaviors.<sup>18-21</sup> Very recently, high-pressure x-ray diffraction (XRD) experiments combined with first-principle calculations demonstrated that  $\beta\text{-Ag}_2\text{Te}$  (phase I) transit

<sup>a</sup>Author to whom correspondence should be addressed. Electronic mail: [sjzhang@iphy.ac.cn](mailto:sjzhang@iphy.ac.cn), [jin@iphy.ac.cn](mailto:jin@iphy.ac.cn)



into phase II, III and IV at 2.4 GPa, 2.8 GPa and 12.8 GPa, respectively, and phase III has been solved to be an orthorhombic structure with the centrosymmetric space group  $Cmca$ .<sup>21</sup> However, the electrical and crystal structure of phase IV have not been determined and the potential effect of the structural phase transitions on the electrical transport properties of  $Ag_2Te$  is still unknown.

To provide insights into the pressure behavior of topological insulator  $Ag_2Te$ , studies of electrical transport properties based on electrical conductivity measurements under high pressures and low temperatures were conducted. We have also performed crystal structure analysis in combination with theoretical calculations on  $Ag_2Te$  to explore both crystal & electronic structural evolutions as a function of pressure. Our results reveal that  $\beta$ - $Ag_2Te$ , which exhibits linear MR behavior due to its topologically non-trivial nature in phase I and phase II, will show distinct electrical behaviors with quadratic MR responses under higher pressures. The first isostructural phase transition from phase I to phase II is attributed to electronic topological transition, which has been observed in  $Bi_2Te_3$ ,  $Sb_2Te_3$  and  $Bi_2Se_3$ .<sup>22–24</sup> The electrical and crystal structures of phase IV are also identified in combination with theoretical calculation.

## II. EXPERIMENTAL DETAILS

High-purity stoichiometric  $Ag_2Te$  (>99.9%) were obtained from Sigma-Aldrich Company. We used diamond anvil cell in combination with Maglab system to investigate the electronic transport properties under pressure at low temperatures. Sample was loaded into a hole with 200  $\mu m$  diameter in a T301 stainless-steel gasket that is preindented from the thickness of 300  $\mu m$  to 60  $\mu m$ . The culet of diamond is 500  $\mu m$  in diameter. The size of the sample was about 100  $\mu m$ \*100  $\mu m$ \*20  $\mu m$ . Cubic boron nitride (cBN) was used as insulating layer between the gasket and the electrodes, while the hexagonal boron nitride (hBN) was used as the pressure transmitting medium. The electrode leads were 18- $\mu m$ -diameter gold wires. Electrical resistance measurements were performed by a standard four-probe technique.

The in situ high-pressure angle-dispersive X-ray diffraction (ADXRD) method is utilized for the structural studies of  $Ag_2Te$  powder samples. The experiments are performed at the National Synchrotron Light Source (NSLS) at Brookhaven National Laboratory with  $\lambda = 0.4134 \text{ \AA}$  using symmetric diamond anvil cells with a pair of 300  $\mu m$  culet diamonds. Silicone oil was used as the pressure transmitting medium to provide a fine quasi-hydrostatic pressure environment. The diffraction patterns are collected using a Mar345 image-plate detector. The two-dimensional diffraction images were studied using the FIT2D software. Data analysis of the high pressure (HP) synchrotron x-ray patterns was performed using the GSAS-EXPGUI package.<sup>25</sup> In both types of experiments pressure was determined by the ruby fluorescence method.<sup>26</sup>

To find the structure of the new phase, we used the evolutionary crystal structure prediction method USPEX,<sup>27,28</sup> which has been successfully used in many previous works, in particular finding new chemistry under pressure.<sup>27,29</sup> For reviews of different crystal structure prediction methods and their comparison, see Ref. 30, USPEX derives its particularly strong efficiency and reliability from a special symmetry-based random structure generation procedure<sup>28</sup> and the use of smart variation operators<sup>28</sup> and fingerprint theory.<sup>31</sup> Structure prediction calculations were performed at 15 GPa for systems with 6, 9, 12 and 18 atoms in the unit cell (2, 3, 4 and 6 formula units, respectively). Each generation consisted of 20-40 structures, depending on system size. The initial generation and 20% of the structures of all subsequent generations were produced randomly, with each structure generated within one of 230 space groups. All structures were relaxed; structure relaxations and enthalpy calculations were done using the VASP code<sup>32</sup> at the level of generalized gradient approximation<sup>33</sup> in conjunction with the all-electron PAW method.<sup>34</sup> The PAW potentials used had [Kr] core (2.4 a.u. radius) for Ag atoms and [Pd] core (radius 2.3 a.u.) for Te atoms. Brillouin zone integration was done with  $\Gamma$ -centered uniform meshes with resolution  $2\pi \times 0.09 \text{ \AA}^{-1}$  and Methfessel-Paxton electronic smearing with  $\sigma = 0.1 \text{ eV}$ , and wave functions were expanded in plane waves with kinetic energy cutoff of 350 eV. After relaxation with the above settings, the total energy was recalculated using a much more stringent k-mesh of resolution  $2\pi \times 0.05 \text{ \AA}^{-1}$ . Self-consistency threshold was  $10^{-4} \text{ eV/cell}$ , and relaxation was done until the enthalpy changed by less than  $10^{-3} \text{ eV/cell}$ . These settings ensured excellent precision and efficiency of the calculations.

After all structures in a generation are relaxed and ranked by enthalpy, the lowest-enthalpy 60% of the structures are used for producing the next generation of structures using heredity (60% of the structures), permutation (10%), soft mutation (10%), and symmetric random generator (20%), and in addition 3-5 different lowest-enthalpy structures are allowed to survive into the next generation.

The calculations of accurate electronic structures are performed using the full-potential linearized augmented plane-wave method,<sup>35</sup> implemented in the package WIEN2K.<sup>36</sup> The exchange-correlation effect was treated with the Perdew, Burke, and Ernzerhof parameterized generalized-gradient approximation.<sup>33</sup> The converged ground states are obtained using the k-mesh of resolution  $2\pi \times 0.02 \text{ \AA}^{-1}$  and  $K_{\text{max}}R_{\text{MT}} = 9.0$ , where  $R_{\text{MT}}$  represents the smallest muffin-tin radius and  $K_{\text{max}}$  is the maximum size of reciprocal-lattice vectors. The muffin-tin radii for both Ag and Te are set to 2.5 Bohr. Spin-orbit coupling was included by a second-variation procedure,<sup>35</sup> where states up to 9 Ry above Fermi level were included in the basis expansion.

### III. RESULTS AND DISCUSSION

Fig. 1(a) shows an overview of resistance in longitudinal scale as a function of temperature at a series of pressure points. At pressures close to ambient, the resistance gradually increases at first by decreasing temperature, which is a typical behavior for semiconductors. The resistance reaches

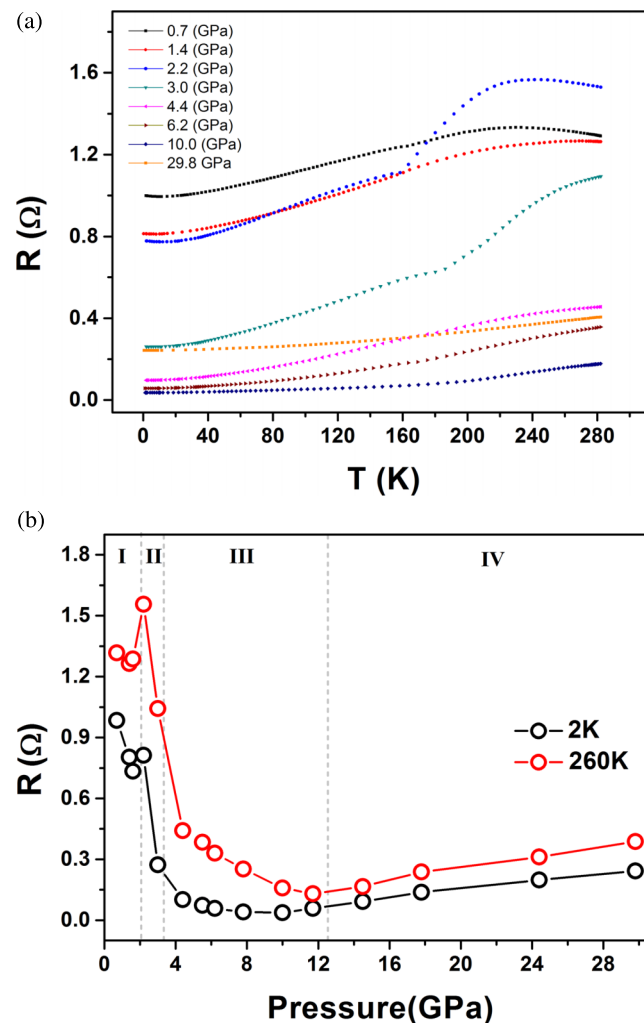


FIG. 1. (a) Temperature dependence of resistance for  $\text{Ag}_2\text{Te}$  from 0.7 to 30.0 GPa. (b) Pressure dependence of resistance for  $\text{Ag}_2\text{Te}$  at 2 K, 260 K. The gray dashed lines are guided to the eye.

a maximum at around 230 K, and then decreases due to the constant effective carrier density and weakening of the phonon scattering contribution. The nonmonotonic curve of  $R(T)$  reflects the behavior of a narrow-gap self-doped degenerate semiconductor, which is in accordance with results in Ref. 8 and 16. Further increasing pressure will dramatically change the electronic structure such that  $\text{Ag}_2\text{Te}$  sample transforms from semiconducting at ambient pressure into metal-like character at high pressures. The experimental results are well repeatable.

The effect of pressure on the electronic properties can be more clearly seen in Fig. 1(b) where the resistance at given temperature is plotted as function of pressure. Upon compression, the resistance decreases with increasing pressure below 1.6 GPa. Then it shows an abrupt increase at around 2 GPa, followed by a sharp decrease with pressure from 2.2 GPa to 3 GPa. The  $p$ -type character at ambient pressure also changes to  $n$ -type character above 2.5 GPa (as shown in Fig. S1).<sup>38</sup> The abnormal increase of resistance probably originates from a pressure-induced electronic topological transition (ETT). The ETT occurs when an extremum of the electronic-band, which is associated to a Van Hove singularity in the electronic density of states (EDOS), crosses the Fermi energy level leading to a strong redistribution of the EDOS near the Fermi energy level.<sup>37</sup> The redistribution of the EDOS leads to a second-order isostructural phase transition, which is closely related to its hole concentration. Following the ETT, a phase transition from phase II to phase III occurs at about 3 GPa, corresponding to the sharp decrease of resistance. After that, the resistance decreases at a much slower rate as the pressure approaches 12 GPa. When pressure is higher than 12.8 GPa, the resistance passes through a minimum and then increases up to the maximal experimental pressure. It is in accordance with the pressure point where structural phase transition from phase III to phase IV was observed in previous paper.<sup>21</sup> The distinct pressure dependence of resistance is clearly related to these four phases since the change of electrical and crystal structures modifies the Fermi surface, which is tightly related to the electrical transport properties of  $\text{Ag}_2\text{Te}$ .

The effect of pressure on the electronic structure can also be reflected from the magnetoresistance (MR). Fig. 2 exhibits the magnetic-field dependence of the magnetoresistance  $\Delta R(B)/R(0) = [R(B) - R(0)]/R(0)$  at 2 K at different pressures. At 1.3 GPa,  $\Delta R(B)/R(0)$  increases with increasing  $H$  and there is no evidence of saturation up to at least 6 T. The value of  $\Delta R(6\text{T})/R(0)$  is 5% and the critical field where MR crosses over from a quadratic to a linear dependence on  $H$  is about 1 T. As the pressure increases to 2.5 GPa, the linear MR behavior is suppressed continuously and shows more quadratic character. Further increasing pressure above 3.3 GPa results in a completely quadratic MR response. The nonsaturating linear MR behaviors were previously observed in  $\text{Ag}_2\text{Te}$  at ambient pressure,<sup>8,9</sup> which may have large contribution from the topological nature.<sup>13</sup> As completely quadratic MR corresponds to the bulk metallic phase III, it is reasonable

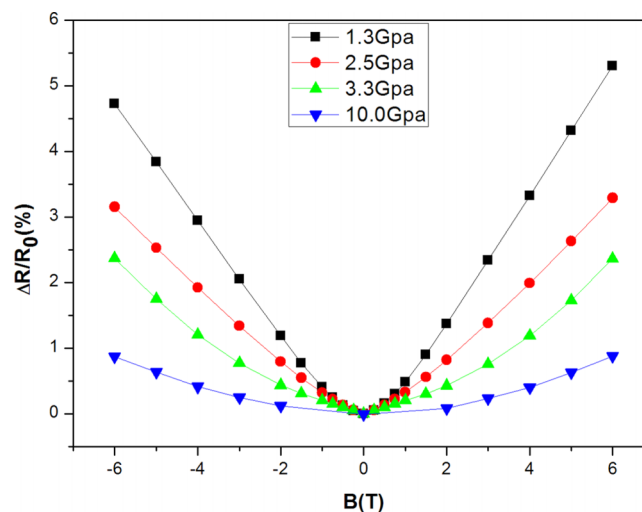


FIG. 2. Normalized magnetoresistance  $\Delta R(B)/R(0) = [R(B) - R(0)]/R(0)$  at  $T=2.0\text{K}$  under transverse magnetic field at a series of pressures. The linear MR will be gradually substituted by quadratic MR as pressure rises.

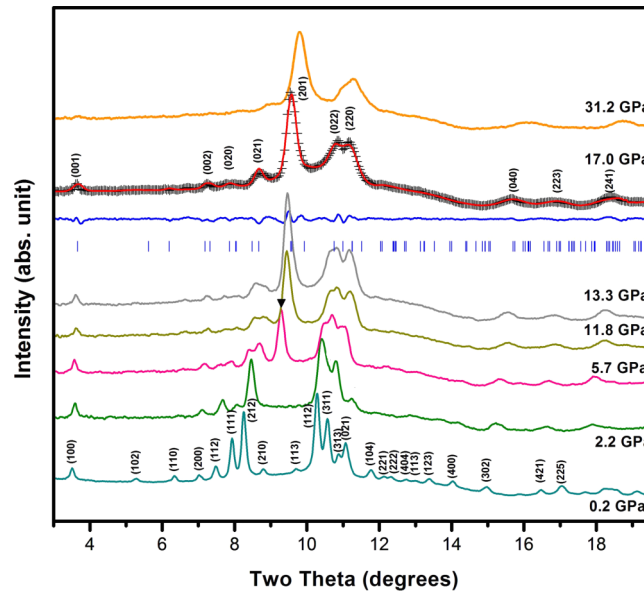


FIG. 3. XRD patterns of  $\text{Ag}_2\text{Te}$  at selected pressure values with an incident wavelength  $\lambda = 0.4314 \text{ \AA}$ .

to infer that the electronic structure of  $\text{Ag}_2\text{Te}$  at high pressures no longer keeps its topological character.

To complement our studies of properties of  $\text{Ag}_2\text{Te}$  under high pressure, we further performed *in situ* high pressure synchrotron X-ray powder diffraction experiments at room temperature with pressure up to 30 GPa. Selected diffraction patterns of  $\text{Ag}_2\text{Te}$  are plotted in Fig. 3. At 0.2 GPa, all the diffraction peaks can be indexed to the structure of ambient  $\beta\text{-Ag}_2\text{Te}$  with space group  $P2_1/c$ . At about 2.2 GPa,  $\text{Ag}_2\text{Te}$  starts the structural phase transformation as some peaks vanished and new peaks appeared (as shown in Fig. S2), and the transition completes at about 3.4 GPa.<sup>38</sup> Note that the transformation from phase III to phase IV completes at 17 GPa. No new peak appears for pressure up to 31.2 GPa (as shown in Fig. S3).<sup>38</sup>

Calculations with the USPEX method reveal the lowest-enthalpy structure found at 16 GPa has space group  $C2/m$  and theoretical cell parameters  $a = 6.08123 \text{ \AA}$ ,  $b = 5.74370 \text{ \AA}$ ,  $c = 6.79746 \text{ \AA}$ ,  $\beta = 105.53^\circ$  with atomic positions Ag (0.58369, 0.5, 0.30281), Ag (0.25, 0.75, 0.0) and Te (0.61390, 0.0, 0.31017). The structure is shown in Fig. 4 and can be described as a compact layered monoclinic structure with triple  $\text{Te}(\text{Ag}_2)\text{-Ag1-Te}(\text{Ag}_2)$  layers similar to those in phase I, II and III.<sup>21</sup>

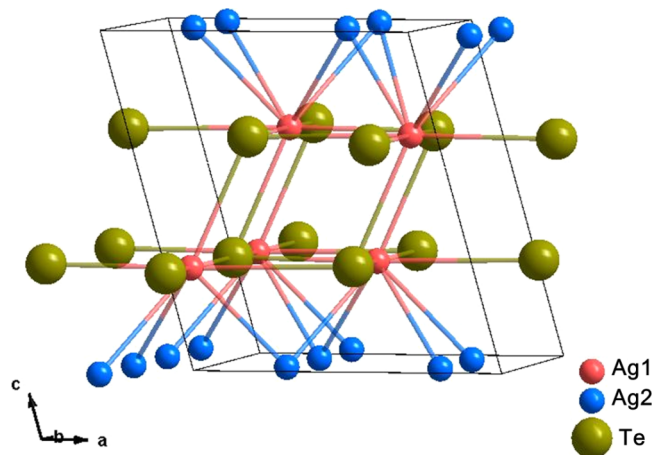


FIG. 4. Schematic view of the crystalline structure of  $\text{Ag}_2\text{Te}$  at phase IV.

TABLE I. Crystal structural data of  $\text{Ag}_2\text{Te}$  II at 17.0 GPa derived from Rietveld refinements in Figure 3. The theoretical lattice parameters and internal atomic sites of  $\text{Ag}_2\text{Te}$  II at 16.0 GPa are listed in parenthesis.

Space group	Lattice parameters ( $\text{\AA}$ , $^\circ$ )	Atom	Atomic coordinates (fractional)		
			x	y	z
$C2/m$	a=6.0631 (6.0812)	Ag1(4i)	0.5588 (0.5837)	0.5	0.2802 (0.3028)
	b=6.0373 (5.7437)	Ag2(4e)	0.25	0.75	0
	c=6.6149 (6.7974)	Te1(4i)	0.5890 (0.6139)	0	0.3241 (0.3102)
	$\beta=103.12$ (105.53)				

From phase III to phase IV, pressure tends to increase the coordination number for Ag1 from five to nine, in which each Ag atom among its 9 nearest neighbors has 5 Te and 4 Ag atoms at distances in the range of 2.7-3.2  $\text{\AA}$ . The X-ray diffraction patterns of  $\text{Ag}_2\text{Te}$  at high pressure are analyzed with Rietveld refinements by using the GSAS program package. A typical refinement result at 17 GPa is shown in Fig. 3 in which the fitted residual Rp and Rpw were 2.72% and 2.05%, respectively. Table I lists the theoretical and experimental cell parameters based on the refinement for comparison. The theoretical profiles fit the experimental data in good way, which enabled us to determine the crystal structure of phase IV unambiguously.

The observed abnormal behaviors in the resistance and MR suggest a pronounced modification of the electronic structure of  $\text{Ag}_2\text{Te}$  under pressure. From Fig. 1 and Fig. 2, we find that phase I is a narrow-gap semiconductor which reveals linear MR behavior. The abrupt increase in the resistance as well as mixed quadratic and linear MR response between 2 to 3 GPa is consistent with the pressure range of the ETT in  $\text{Ag}_2\text{Te}$ . Based on recent theoretical calculations of the electronic structure,<sup>21</sup> isostructural phase II maintains its topological nontrivial surface state while the bulk changes to semimetal. That is, the bulk metallic properties dominate the surface properties, resulting in some degree of quadratic character in the MR behavior. After structural phase transition, phase III behaves like metals with quadratic MR response. Note that the resistance of  $\text{Ag}_2\text{Te}$  at phase III decreases smoothly with increasing pressure, and after passing through a minimum at around 12 GPa, starts to increase in phase IV after the third phase transition.

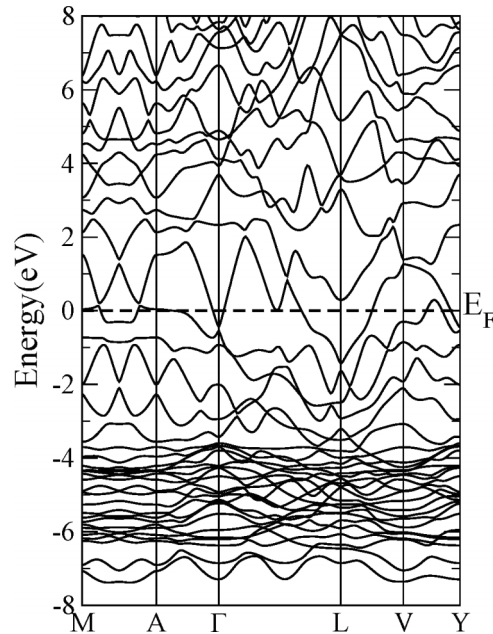


FIG. 5. Electronic band structure of  $\text{Ag}_2\text{Te}$  at phase IV based on experimental measurements of the crystal lattice. A metallic state for phase IV is obtained.

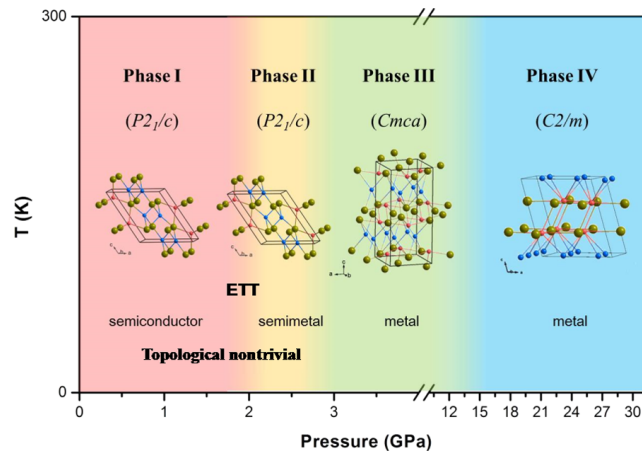


FIG. 6. Pressure-temperature phase diagram of  $\text{Ag}_2\text{Te}$  polymorphs.

An analysis of the densities of states suggests that phase III is a bulk metal.<sup>21</sup> To further clarify the nature of metallic behavior of phase IV, we studied the electronic structures using first-principles calculations based on density functional theory and the generalized gradient approximation with spin orbital coupling (SOC). The band structure of phase IV at experimentally refined crystal structure is plotted in Fig. 5, in which one can clearly see the metallic feature with complex multibands crossing the Fermi level. The metallicity of phase IV identified from the band structure is in good agreement with our experimental measurements. Although this system is a metallic phase, it has local band gap everywhere in entire Brillouin zone. Therefore, the  $Z_2$  topological invariants can be well defined. The calculated  $Z_2$  invariants (0;000) indicate that this high-pressure phase is a metal.

In order to have a more intuitive understanding of the structural and electronic evolution of  $\text{Ag}_2\text{Te}$  under pressure, we plot in Fig. 6 the pressure-temperature phase diagram based on the results mentioned above. Phase I and phase II which have topological nontrivial surface states can only stabilize in a narrow pressure range. At pressure above 3 GPa, phase III and phase IV appears in sequence, converting  $\text{Ag}_2\text{Te}$  from topological insulator into topologically trivial metal.

In summary, the high pressure structure of  $\text{Ag}_2\text{Te}$  at phase IV was analyzed based on experimental results in combination with theoretical optimization to be a monoclinic layered structure (space group  $C2/m$ ). Electrical conductivity measurements show that semimetal phase II preserve its topological nontrivial nature with mixed quadratic and linear MR response, while both the phase III and IV are bulk metals with non-saturating quadratic MR behavior.

## ACKNOWLEDGMENTS

This work was supported by NSF & MOST of China through research projects. We are grateful to Dr. Z.Q.Chen for the help in doing experiments at NSLS. A.R.O. gratefully acknowledges support from the National Science Foundation (grant EAR-1114313) and DARPA (grant N66001-10-1-40373). Calculations were performed at the Joint Supercomputer Center of the Russian Academy of Sciences and on the Skif supercomputer (Moscow State University).

<sup>1</sup> I. Karakaya and W. T. Thompson, *J. Phase Equilib.* **12**, 56 (1991).

<sup>2</sup> J. B. Boyce and B. A. Huberman, *Phys. Rep.* **51**, 189 (1979).

<sup>3</sup> R. Dalven, *Phys. Rev. Lett.* **16**, 311 (1966).

<sup>4</sup> R. Dalven and R. Gill, *Phys. Rev.* **159**, 645 (1967).

<sup>5</sup> P. Junod *et al.*, *Philos. Mag.* **36**, 941 (1977).

<sup>6</sup> S. A. Aliev and F. F. Aliev, *Izv. Akad. Nauk SSSR, Neorg. Mater.* **21**, 1869 (1985).

<sup>7</sup> M. Fujikane, K. Kurosaki, H. Muta, and S. Yamanaka, *J. Alloys Compd.* **393**, 299 (2005).

<sup>8</sup> R. Xu, A. Hussman, T. F. Rosenbaum, M.-L. Saboungi, J. E. Enderby, and P. B. Littlewood, *Nature (London)* **390**, 57 (1997).

<sup>9</sup> A. Husmann, J. B. Betts, G. S. Boebinger, A. Migliori, T. F. Rosenbaum, and M. L. Saboungi, *Nature (London)* **417**, 421 (2002).

<sup>10</sup> A. A. Abrikosov, *Phys. Rev. B* **58**, 2788 (1998).

- <sup>11</sup> A. A. Abrikosov, *Phys. Rev. B* **60**, 4231 (1999).
- <sup>12</sup> M. M. Parish and P. B. Littlewood, *Nature (London)* **426**, 162 (2003).
- <sup>13</sup> W. Zhang, R. Yu, W. X. Feng, Y. G. Yao, H. M. Weng, X. Dai, and Z. Fang, *Phys. Rev. Lett.* **106**, 156808 (2011).
- <sup>14</sup> A. Sulaev, P. Ren, B. Xia, Q. H. Lin, T. Yu, C. Qiu, S.-Y. Zhang, M.-Y. Han, Z. P. Li, W. G. Zhu, Q. Wu, Y. P. Feng, L. Shen, S.-Q. Shen, and L. Wang, *AIP Adv.* **3**, 032123 (2013).
- <sup>15</sup> J. L. Zhang, S. J. Zhang, H. M. Weng, W. Zhang, L. X. Yang, Q. Q. Liu, S. M. Feng, X. C. Wang, R. C. Yu, L. Z. Cao, L. Wang, W. G. Yang, H. Z. Liu, W. Y. Zhao, S. C. Zhang, X. Dai, Z. Fang, and C. Q. Jin, *Proc. Natl. Acad. Sci. U.S.A.* **108**, 24 (2011).
- <sup>16</sup> J. Zhu, J. L. Zhang, P. P. Kong, S. J. Zhang, X. H. Yu, J. L. Zhu, Q. Q. Liu, X. Li, R. C. Yu, R. Ahuja, W. G. Yang, G. Y. Shen, H. K. Mao, H. M. Weng, X. Dai, Z. Fang, Y. S. Zhao, and C. Q. Jin, *Sci. Rep.* **3**, 2016 (2013).
- <sup>17</sup> P. P. Kong, J. L. Zhang, S. J. Zhang, J. Zhu, Q. Q. Liu, R. C. Yu, Z. Fang, C. Q. Jin, W. G. Yang, X. H. Yu, J. L. Zhu, and Y. S. Zhao, *J. Phys.: Condens. Matter* **25**, 362204 (2013).
- <sup>18</sup> M. D. Banus and M. C. Finn, *J. Electrochem. Soc.: SOLID STATE SCIENCE* **116**, 91 (1969).
- <sup>19</sup> M. Lee, T. F. Rosenbaum, M.-L. Saboungi, and H. S. Schnyders, *Phys. Rev. Lett.* **88**, 066602 (2002).
- <sup>20</sup> Yuhang Zhang, Yan Li, Yanmei Ma, Yuwei Li, Guanghui Li, Xuecheng Shao, Hui Wang, Tian Cui, Xin Wang, and Pinwen Zhu, *Scientific Reports* **5**, 14681 (2015).
- <sup>21</sup> Z. Zhao, S. Wang, H. Zhang, and W. L. Mao, *Phys. Rev. B* **88**, 024120 (2013).
- <sup>22</sup> O. Gomis, R. Vilaplana, F. J. Manjón, P. Rodríguez-Hernández, E. Pérez-González, A. Muñoz, V. Kucek, and C. Drasar, *Phys. Rev. B* **84**, 174305 (2011).
- <sup>23</sup> R. Vilaplana, O. Gomis, F. J. Manjón, A. Segura, E. Pérez-González, P. Rodríguez-Hernández, A. Muñoz, J. González, V. Marín-Borrás, V. Muñoz-Sanjose, C. Drasar, and V. Kucek, *Phys. Rev. B* **84**, 104112 (2011).
- <sup>24</sup> Rosario Vilaplana, D. Santamaría-Pérez, O. Gomis, F. J. Manjón, J. González, A. Segura, A. Muñoz, P. Rodríguez-Hernández, E. Pérez-González, V. Marín-Borrás, V. Muñoz-Sanjose, C. Drasar, and V. Kucek, *Phys. Rev. B* **84**, 184110 (2011).
- <sup>25</sup> A. C. Larson and R. B. Von Dreele, Los Alamos National Laboratory Report No. LAUR, 86-748, 1994.
- <sup>26</sup> H. K. Mao, P. M. Bell, J. W. Shaner, and D. J. Steinberg, *J. Appl. Phys.* **49**, 3276 (1978).
- <sup>27</sup> A. R. Oganov and C. W. Glass, *J. Phys.: Condens. Matter* **20**, 064210 (2008).
- <sup>28</sup> A. O. Lyakhov, A. R. Oganov, and M. Valle, *Comp. Phys. Commun.* **181**, 1623 (2010).
- <sup>29</sup> M. Martínez-Canales, A. R. Oganov, Y. Ma, Y. Yan, A. O. Lyakhov, and A. Bergara, *Phys. Rev. Lett.* **102**, 087005 (2009).
- <sup>30</sup> *Modern Methods of Crystal Structure Prediction*, edited by A. R. Oganov (Berlin: Wiley-VCH, 2010), ISBN: 978-3-527-40939-6.
- <sup>31</sup> A. R. Oganov and M. Valle, *J. Chem. Phys.* **130**, 104504 (2009).
- <sup>32</sup> G. Kresse and J. Furthmüller, *Phys. Rev. B* **54**, 11169 (1996).
- <sup>33</sup> J. P. Perdew, K. Burke, and M. Ernzerhof, *Phys. Rev. Lett.* **77**, 3865 (1996).
- <sup>34</sup> G. Kresse and D. Joubert, *Phys. Rev. B* **59**, 1758 (1999).
- <sup>35</sup> D. J. Singh, "Planewaves," *Pseudopotentials and the LAPW Method* (Kluwer Academic, Boston, 1994).
- <sup>36</sup> P. Blaha, K. Schwarz, G. Madsen, D. Kvaniscka, and J. Luitz, *Wien2k, An Augmented Plane Wave Plus Local Orbitals Program for Calculating Crystal Properties* (Vienna University of Technology, Vienna, Austria, 2001).
- <sup>37</sup> I. M. Lifshitz, *Sov. Phys. JETP* **11**, 1130 (1960).
- <sup>38</sup> See supplementary material at <http://dx.doi.org/10.1063/1.4960606> for the evolution of carrier under pressure and XRD patterns of Ag<sub>2</sub>Te at each pressure point.